Acta Crystallographica Section B
Structural Science
ISSN 0108-7681

Temperature-dependent neutron powder diffraction study of the $Ba(OD)_2$ polymorphs: a new low-temperature phase

Alexandra Friedrich,[a]* Martin Kunz[a] and Emmanuelle Suard[b]

[a]Laboratorium für Kristallographie, ETH Zentrum, Sonneggstrasse 5, CH-8092 Zürich, Switzerland, and [b]Institut Laue–Langevin, BP 156X, 38042 Grenoble CEDEX 9, France

Correspondence e-mail: alexandra@kristall.erdw.ethz.ch

Received 19 April 2001
Accepted 16 August 2001

The structural behaviour of both low-temperature β- and high-temperature α-$Ba(OD)_2$, barium dihydroxide-*d*, was investigated at temperatures between 10 and 552 K by neutron powder diffraction. While the β phase ($P2_1/n$) remains stable to the lowest temperature investigated, the quenchable α phase (*Pnma*) shows a reversible orthorhombic-to-monoclinic phase transition between 100 and 150 K. The structure of the new α_m phase ($P2_1/n$) is quite similar to that of the α phase. This behaviour is unusual as a metastable phase transforms to another metastable phase. The *Pnma* $\leftrightarrow$ $P2_1/n$ low-temperature phase transition is driven by an order–disorder mechanism, mainly caused by one of the D atoms, which is disordered on positions off the mirror plane, mimicking a special position on the mirror plane in the orthorhombic phase. Refinements of the α phase above the phase transition indicate this disorder across the mirror plane through a conspicuously high isotropic displacement parameter if compared to the other D atoms. At low temperature the energy of the vibration is lowered and the D atom is frozen at a general position in a correlated way, thus violating the mirror plane and reducing the space-group symmetry.

1. Introduction

Two modifications of $Ba(OH)_2$ have been described in the literature (Michaud, 1968; Buck & Bärnighausen, 1968; Lutz *et al.*, 1969), a low-temperature β phase and a high-temperature α phase. Several studies dealt with the thermal decomposition of barium hydroxide and its hydrates. Thermogravimetric (TG) and differential thermal analysis (DTA) curves between 273 and 1173 K were measured by Habashy & Kolta (1972), TG by Michaud (1968) and thermoanalytical measurements (DTA, TG, DTG, differential thermal gravimetry, high-temperature X-ray diffraction and high-temperature Raman scattering) on the hydrates of barium hydroxide by Lutz, Eckers, Christian & Engelen (1981) and Lutz, Eckers, Schneider & Haeuseler (1981). Further DSC (differential scanning calorimetry) and DTA data were reported by Maneva-Petrova & Nikolova (1985), and standard enthalpies of formation and heat capacities by Konings *et al.* (1988, 1990). The β-to-α phase transition was studied in detail by calorimetric, X-ray powder diffraction, IR spectroscopic and thermal analysis (DSC) techniques by Cordfunke *et al.* (1996). The phase transition was reported to occur at 526 (2) K (Cordfunke *et al.*, 1996). It is irreversible and quenchable, which means that the α phase only successively transforms back to the β phase at long storage times or extremely slow

cooling rates. The back transformation can be catalysed by the presence of small amounts of water. Therefore, the α phase is metastable at room temperature in the absence of humidity (Cordfunke *et al.*, 1996). The crystal structure of α-$Ba(OH)_2$ was solved from single-crystal X-ray measurements (Lüke, 1973), with only calculated H sites in the model. In 1997 the crystal structure of β-$Ba(OD)_2$ as well as the D sites of α-$Ba(OD)_2$ were located from neutron powder data by Denzinger (1997). The polymorphs of $Ba(OH)_2$ were also investigated by IR and Raman spectroscopy (Lutz, Eckers, Sneider & Haeuseler, 1981). Structural *in situ* high-pressure powder diffraction studies of both polymorphs revealed several new high-pressure polymorphs (Friedrich *et al.*, 2001).

In this study β- and α-$Ba(OD)_2$ have been structurally investigated at different temperatures between 552 and 10 K (Fig. 1). A new metastable low-temperature polymorph was found. We derived the temperature-dependent structural behaviour, which revealed the driving mechanism for the α–α_m phase transition. Further investigations on this phase transition are ongoing by the use of spectroscopic and diffraction methods.

2. Experimental

Pure powder of the β-modification of deuterated barium dihydroxide, β-$Ba(OD)_2$, was synthesized using BaO and D_2O as the starting materials. D_2O was heated up to ~363 K under a slow stream of nitrogen to increase the solubility of BaO, which was added up to saturation. Then the solution was filtered to remove small amounts of barium carbonate and was put in a desiccator. Small crystals of deuterated barium hydroxide octahydrate, $Ba(OD)_2{\cdot}8D_2O$, were grown by slow cooling of the hot solution. The crystals were filled in a corundum crucible, which was placed in a quartz-glass tube under a nitrogen atmosphere. The sample was dried by slow evacuation and finally heated to 373 K for dehydration. The tube was evacuated and heated in several cycles until a pure powder of β-$Ba(OD)_2$ was obtained. Approximately 10 cm^3 of the powdered sample were loaded into two vanadium cans under a helium atmosphere, using a gold wire for sealing.

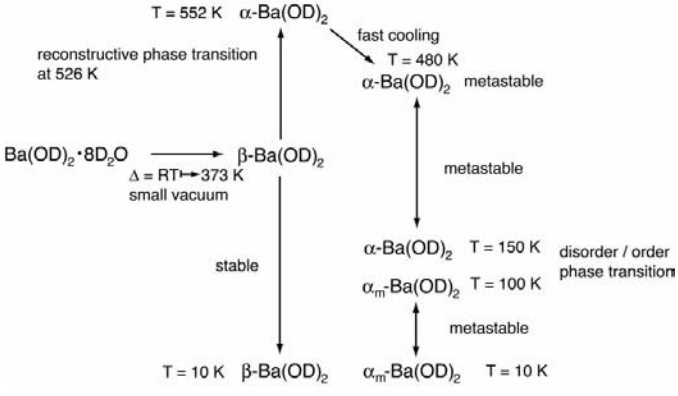

Figure 1
Comprehensive overview of the phase transitions in the system $Ba(OD)_2$.

Neutron powder diffraction data were collected on the D2B high-resolution two-axis diffractometer at the high-flux reactor of the Institut Laue–Langevin (ILL), Grenoble, France. Powder patterns were measured at 480, 420, 300, 250, 200, 150, 100, 50 and 10 K for β-$Ba(OD)_2$, at 552, 480, 200 and 150 K for α-$Ba(OD)_2$, and at 100, 50 and 10 K for new α_m-$Ba(OD)_2$. The samples were equilibrated at temperatures between 10 and 300 K for 10 min each before measurement and at higher temperatures for 15–30 min. A wavelength of 1.594 Å was selected with a (335)Ge monochromator at a take-off angle of 135°. The (angle-dispersive) data were collected in several scans in the range $0 \leq 2\theta \leq 160°$ with ~50 steps of 0.05° stepsize in 2θ, using 64 detectors at 2.5° intervals. The vanadium can was mounted on the centre stick of a top-loading ILL gas-flow helium cryofurnace or cryostat for all measurements.

The structures were refined using the *General Structure Analysis System* (*GSAS*; Larson & Von Dreele, 1994). Starting values in the refinements for β-$Ba(OD)_2$ and α-$Ba(OD)_2$ were those reported by Denzinger (1997) and Lüke (1973), respectively. The cryostat produced a single aluminium reflection between 145 and 148° 2θ, which was excluded from the diffraction patterns during refinement. Peak splitting and

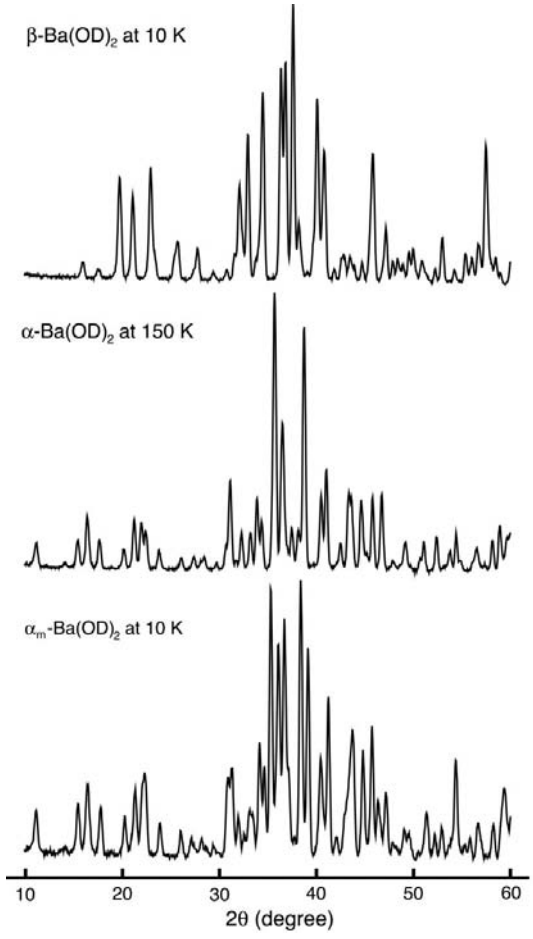

Figure 2
Powder diffraction patterns of β-, α- and α_m-$Ba(OD)_2$ in a selected 2θ range.

Table 1
Unit-cell parameters and residual values (%) of β-$Ba(OD)_2$.

RT = room temperature.

Parameters	RT	480 K	420 K	300 K	250 K
a (Å)	9.4098 (3)	9.4881 (2)	9.4576 (3)	9.4084 (2)	9.3912 (2)
b (Å)	7.9101 (3)	7.9527 (2)	7.9390 (2)	7.9085 (1)	7.8958 (1)
c (Å)	6.7759 (2)	6.7985 (2)	6.7893 (2)	6.7748 (1)	6.7682 (1)
β (°)	95.765 (2)	95.912 (1)	95.869 (2)	95.757 (1)	95.720 (1)
V (Å^3)	501.80 (3)	510.26 (2)	507.09 (2)	501.55 (1)	499.37 (2)
χ^2	3.807	2.283	2.461	2.454	1.779
R_{wp}	4.31	2.83	3.36	2.35	2.70
R_p	3.07	2.25	2.59	1.87	2.14
$R(F^2)$	5.17	5.79	5.51	3.17	2.81

Parameters	200 K	150 K	100 K	50 K	10 K
a (Å)	9.3772 (2)	9.3652 (2)	9.3561 (2)	9.3506 (2)	9.3489 (1)
b (Å)	7.8850 (1)	7.8763 (1)	7.8696 (1)	7.8659 (1)	7.8649 (1)
c (Å)	6.7629 (1)	6.7581 (1)	6.7547 (1)	6.7528 (1)	6.7525 (1)
β (°)	95.689 (1)	95.667 (1)	95.656 (1)	95.655 (1)	95.655 (1)
V (Å^3)	497.58 (1)	496.06 (1)	494.92 (1)	494.25 (1)	494.08 (1)
χ^2	1.703	1.796	1.797	1.844	2.114
R_{wp}	2.64	2.71	2.71	2.74	2.69
R_p	2.10	2.13	2.13	2.18	2.12
$R(F^2)$	2.41	2.37	2.20	2.21	2.26

$\chi^2 = \sum w(I_o - I_c)^2/(N_{obs} - N_{var})$, $R_{wp} = [\sum w(I_o - I_c)^2/\sum w(I_o^2)]^{1/2}$, $R_p = \sum|I_o - I_c|/\sum I_o$, $R(F^2) = \sum|F_o^2 - SF_c^2|/\sum|F_o^2|$; where w = weight, S = scale factor, N_{obs} = No. of observations, N_{var} = No. of variables.

Table 2
Unit-cell parameters and residual values (%) of α-$Ba(OD)_2$.

Parameters	552 K	480 K	200 K	150 K	100 K	50 K	10 K
a (Å)	11.1191 (5)	11.0818 (4)	10.9789 (3)	10.9577 (3)	7.0832 (2)	7.0826 (2)	7.0825 (2)
b (Å)	16.6694 (9)	16.6025 (5)	16.4317 (4)	16.4138 (5)	10.8967 (3)	10.8730 (3)	10.8701 (3)
c (Å)	7.1420 (4)	7.1255 (2)	7.0784 (2)	7.0737 (2)	16.4306 (5)	16.4338 (4)	16.4349 (4)
β (°)					91.060 (2)	91.309 (2)	91.333 (2)
V (Å^3)	1323.8 (1)	1310.99 (7)	1276.96 (6)	1272.26 (6)	1267.96 (6)	1265.22 (5)	1264.94 (5)
χ^2	1.772	2.335	3.194	3.236	2.310	1.751	1.987
R_{wp}	3.21	3.23	3.92	3.94	3.30	2.86	3.06
R_p	2.54	2.53	3.11	3.13	2.65	2.25	2.45
$R(F^2)$	6.43	9.42	6.00	5.20	2.95	2.15	2.13

additional peaks at higher 2θ angles indicated a loss of symmetry elements and a reduction in space-group symmetry for α_m-$Ba(OD)_2$ (Fig. 2). Systematic absences and the supergroup–subgroup relationship suggest the space group $P2_1/n$ as the highest symmetry possible. Structural models were refined by varying lattice parameters and all atomic positions with isotropic displacement parameters. For the refinement of α-$Ba(OD)_2$ at 150 K the isotropic displacement parameter of the Ba1 atom was fixed to a value of 0.002 Å^2. The background was modelled by a shifted Chebyshev function (function 1; Larson & Von Dreele, 1994) using 15 refinable background coefficients for most diffraction patterns. Data of α_m-$Ba(OD)_2$ at and below 150 K were refined with 24–36 coefficients. Scale factor and profile functions were also refined. The Gaussian and Lorentzian line-shape parameters (GU, GV, GW and LX), as well as the asymmetric parameter of a pseudovoigt function were varied during refinement of the β phase, and GW, LY and the asymmetric term for the α and α_m phases.

Unit-cell parameters and the final discrepancy factors are summarized in Tables 1 and 2. Atomic parameters and isotropic displacement factors are given in Tables 3–5. Selected interatomic distances are given in Tables 6 and 7. Hydrogen-bond parameters are listed in Tables 8–10.[1]

3. Results and discussion

3.1. Crystal structures

The β phase of $Ba(OD)_2$ is the stable low-temperature phase and crystallizes in space group $P2_1/n$. The crystal structure can be described by a distorted hexagonal close-packing of Ba atoms in an AB stacking sequence (Denzinger, 1997; Bärnighausen *et al.*, 1997). All tetrahedral and octahedral voids are occupied by O or D atoms. Two of four hydroxyl ions are coordinated by distorted barium octahedra, the others by distorted trigonal bipyramids. Two barium sites are distinguished, Ba1 coordinated by eight [8] and Ba2 by seven [7 + 1] O atoms (Fig. 3*a*). The face-linked polyhedra form serrated double chains along the b axis. Those chains are connected *via* edges along the a axis and form interstitials within a sheet, which are occupied by D atoms. The sheets are interconnected *via* polyhedral edges or corners. Hydrogen bonds exist within the cavities. The D1, D2 and D4 atoms are part of the hydrogen bonds within the coordination polyhedron of the Ba1 atom.

The high-temperature α phase of $Ba(OD)_2$ crystallizes in space group *Pnma*. The crystal structure (Lüke, 1973; Denzinger, 1997) shows three distinct barium sites, Ba1 coordinated by [8], Ba2 by [7 + 1] and Ba3 by [9] hydroxyl groups (Fig. 3*b*). An additional empty nine-coordinated interstitial holds hydrogen-bonded D atoms. The hydroxyl ions are one-sided surrounded by Ba atoms, opposite to the hydrogen proton. One of six hydroxyl ions (O2—D2) is coordinated by three Ba atoms and forms the top of a trigonal pyramid. Three hydroxyl ions are coordinated by strongly distorted barium tetrahedra and two by tetragonal barium pyramids. The D5 atom is located on the edges of the Ba1

[1] Supplementary data for this paper are available from the IUCr electronic archives (Reference: OS0074). Services for accessing these data are described at the back of the journal.

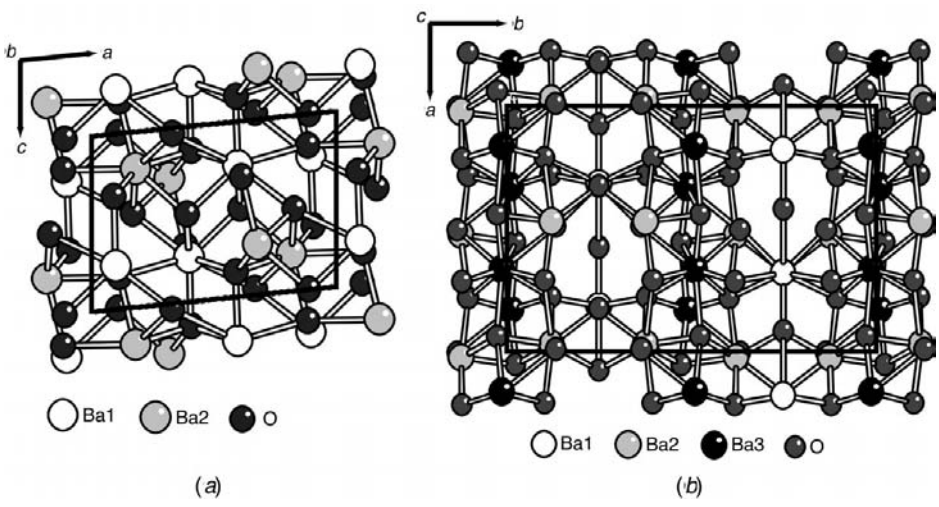

Figure 3
Crystal structures of (*a*) β-Ba(OD)$_2$ and (*b*) α-Ba(OD)$_2$, projected along the *b* and *c* axes, respectively. Only the framework of the Ba and O atoms is drawn.

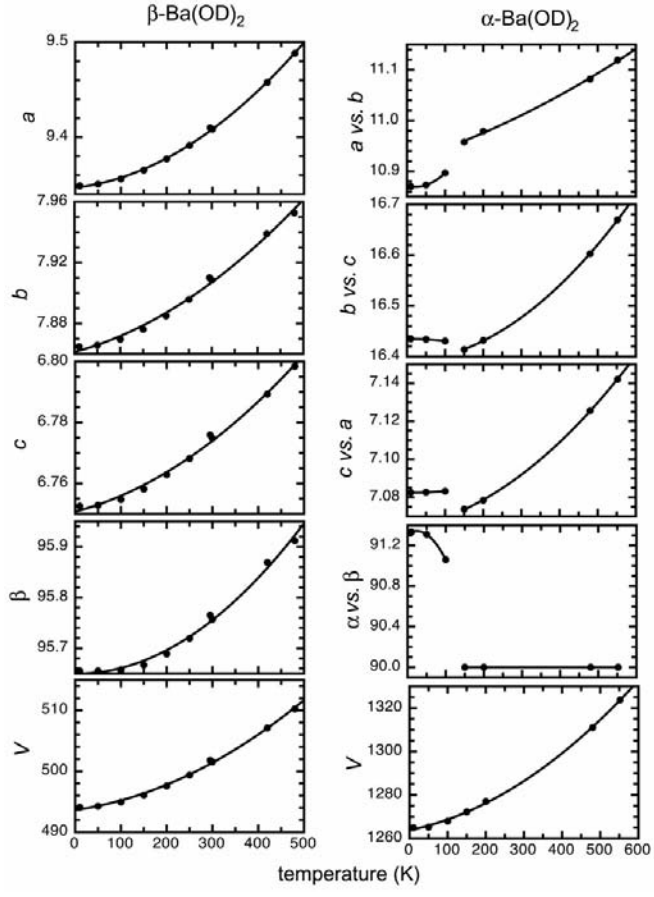

Figure 4
Unit-cell parameters of β- and α-Ba(OD)$_2$ with temperature. Unit-cell axes are given in Å, volumes in Å^3. A clear discontinuity between 100 and 150 K indicates the α-to-α_m phase transition. Appropriate axes designations are given for the high-temperature α phase *versus* the low-temperature α_m phase.

polyhedron and forms a weak hydrogen bond between the O atoms. The D1 and D6 atoms are also parts of weak hydrogen bonds within the coordination polyhedra of the Ba1 and Ba3 atoms, respectively.

3.2. Phase transitions

The investigation of the β phase of Ba(OD)$_2$ between 480 and 10 K does not show any anomalous behavior (Fig. 4). The unit-cell volume as well as the unit-cell parameters [$P2_1/n$; a = 9.3772 (2), b = 7.8850 (1), c = 6.7629 (1) Å, β = 95.6888 (9)° at 200 K] decrease slightly with decreasing temperature. Between 480 and 552 K the β phase transforms to the α phase [*Pnma*; a = 10.9789 (3), b = 16.4317 (4), c = 7.0784 (2) Å at 200 K], as reported previously (Cordfunke *et al.*, 1996) and remains metastable upon cooling. α-Ba(OD)$_2$ also shows a slight decrease of the unit-cell volume with decreasing temperature. The unit-cell parameters, however, show distinct discontinuities between 150 and 100 K, which indicate the low-temperature α-to-α_m phase transition. While the a axis is shortened more towards lower temperature, the b and c axes expand and the α angle increases, transforming to a monoclinic β angle [$P2_1/n$; a = 7.0832 (2), b = 10.8967 (3), c = 16.4306 (5) Å, β = 91.060 (2)° at 100 K]. The phase transition is explained by an orthorhombic-to-monoclinic symmetry change (*Pnma* $\rightarrow$ $P2_1/n$ 1 1) and a transformation to standard settings by applying the transformation matrix [0, 1, 0; 0, 0, 1; 1, 0, 0]. It is very unusual that a metastable high-temperature phase shows a phase transition towards another metastable phase at low temperature. It would be expected that the high-temperature phase transformed back to the stable low-temperature phase, in this case the β phase. Instead a new α_m phase is formed. The cooling rate from the 480 K measurement to 10 K was as fast as possible, taking about 2.5 to 3 h for whole equilibration even in the low-temperature range, maybe preventing the α phase turning back to the β phase, but transforming to the α_m phase. On raising the temperature the α_m phase reconverts to the α phase, which is also unusual. It can be explained by the close relationship between the structures of the orthorhombic and monoclinic α phases, which is energetically preferable, while the structure of the β phase is quite different and needs more activation energy for formation. It is not possible to gain exact information on the order of the phase transition from these data, as the steps in temperature were too large.

3.3. Structural correlations

3.3.1. β–α phase. As this is a reconstructive phase transition it is not surprising that the α phase can be obtained as meta-

Table 3
Atom positions and atomic displacement parameters of β-$Ba(OD)_2$.

Site	x	y	z	U_{eq}
Room temperature				
Ba1	0.5990 (5)	0.6394 (6)	0.2505 (7)	0.012 (1)
Ba2	0.1793 (4)	0.5499 (5)	0.2170 (7)	0.0090 (9)
O1	0.8802 (4)	0.4871 (5)	0.1769 (7)	0.0133 (9)
O2	0.4108 (4)	0.3595 (6)	0.1439 (6)	0.0139 (9)
O3	0.6052 (4)	0.3451 (6)	0.4916 (7)	0.016 (1)
O4	0.1659 (5)	0.2949 (5)	0.4662 (7)	0.021 (1)
D1	0.8828 (5)	0.5298 (6)	0.3094 (7)	0.036 (1)
D2	0.4702 (4)	0.3484 (5)	0.2682 (7)	0.0275 (9)
D3	0.6258 (5)	0.2365 (6)	0.4394 (7)	0.031 (1)
D4	0.1029 (5)	0.2462 (6)	0.5475 (9)	0.036 (1)
480 K				
Ba1	0.5999 (3)	0.6371 (4)	0.2534 (5)	0.0206 (8)
Ba2	0.1810 (3)	0.5446 (4)	0.2139 (5)	0.0154 (7)
O1	0.8851 (3)	0.4842 (4)	0.1797 (6)	0.0286 (8)
O2	0.4086 (3)	0.3568 (4)	0.1418 (5)	0.0243 (8)
O3	0.6092 (3)	0.3466 (5)	0.4979 (6)	0.0335 (9)
O4	0.1693 (3)	0.2920 (4)	0.4643 (5)	0.0277 (9)
D1	0.8840 (4)	0.5279 (5)	0.3092 (6)	0.059 (1)
D2	0.4681 (3)	0.3476 (4)	0.2636 (5)	0.0447 (9)
D3	0.6266 (4)	0.2432 (5)	0.4446 (6)	0.055 (1)
D4	0.1080 (4)	0.2474 (5)	0.5479 (7)	0.057 (1)
420 K				
Ba1	0.5996 (4)	0.6382 (5)	0.2519 (6)	0.0176 (9)
Ba2	0.1802 (4)	0.5474 (4)	0.2158 (6)	0.0127 (8)
O1	0.8827 (4)	0.4857 (5)	0.1783 (6)	0.0224 (8)
O2	0.4096 (4)	0.3578 (5)	0.1430 (5)	0.0193 (8)
O3	0.6075 (4)	0.3451 (5)	0.4952 (6)	0.0253 (9)
O4	0.1675 (4)	0.2933 (5)	0.4642 (6)	0.025 (1)
D1	0.8832 (4)	0.5279 (5)	0.3099 (7)	0.048 (1)
D2	0.4684 (4)	0.3480 (5)	0.2650 (6)	0.0370 (9)
D3	0.6256 (4)	0.2398 (5)	0.4409 (6)	0.043 (1)
D4	0.1058 (4)	0.2470 (5)	0.5474 (8)	0.049 (1)
300 K				
Ba1	0.6018 (2)	0.6396 (3)	0.2519 (3)	0.0111 (5)
Ba2	0.1810 (2)	0.5475 (3)	0.2158 (3)	0.0110 (5)
O1	0.8825 (2)	0.4866 (3)	0.1772 (3)	0.0140 (5)
O2	0.4108 (2)	0.3594 (3)	0.1444 (3)	0.0147 (5)
O3	0.6068 (2)	0.3462 (3)	0.4953 (3)	0.0163 (5)
O4	0.1662 (2)	0.2960 (3)	0.4646 (3)	0.0181 (5)
D1	0.8844 (2)	0.5299 (3)	0.3101 (4)	0.0354 (6)
D2	0.4697 (2)	0.3494 (3)	0.2702 (3)	0.0258 (4)
D3	0.6249 (2)	0.2383 (3)	0.4424 (3)	0.0323 (6)
D4	0.1041 (3)	0.2444 (3)	0.5505 (4)	0.0353 (6)
250 K				
Ba1	0.6027 (3)	0.6400 (3)	0.2512 (4)	0.0084 (5)
Ba2	0.1813 (2)	0.5483 (3)	0.2160 (4)	0.0091 (5)
O1	0.8824 (2)	0.4870 (3)	0.1766 (4)	0.0113 (5)
O2	0.4114 (2)	0.3601 (3)	0.1452 (3)	0.0125 (5)
O3	0.6066 (2)	0.3464 (3)	0.4947 (4)	0.0130 (5)
O4	0.1654 (2)	0.2962 (3)	0.4656 (4)	0.0139 (5)
D1	0.8847 (2)	0.5304 (3)	0.3104 (4)	0.0299 (6)
D2	0.4702 (2)	0.3494 (3)	0.2709 (3)	0.0231 (5)
D3	0.6249 (2)	0.2370 (3)	0.4426 (3)	0.0280 (6)
D4	0.1028 (3)	0.2434 (3)	0.5507 (4)	0.0306 (6)
200 K				
Ba1	0.6029 (2)	0.6406 (3)	0.2503 (3)	0.0065 (5)
Ba2	0.1816 (2)	0.5482 (3)	0.2158 (4)	0.0070 (4)
O1	0.8823 (2)	0.4878 (3)	0.1763 (3)	0.0094 (4)
O2	0.4119 (2)	0.3604 (3)	0.1452 (3)	0.0092 (4)
O3	0.6067 (2)	0.3462 (3)	0.4942 (3)	0.0096 (4)
O4	0.1649 (2)	0.2964 (3)	0.4651 (3)	0.0117 (5)
D1	0.8846 (2)	0.5308 (3)	0.3104 (4)	0.0270 (5)
D2	0.4708 (2)	0.3494 (3)	0.2721 (3)	0.0209 (4)
D3	0.6246 (2)	0.2362 (3)	0.4423 (3)	0.0257 (6)
D4	0.1022 (2)	0.2431 (3)	0.5514 (4)	0.0272 (6)

Table 3 (continued)

Site	x	y	z	U_{eq}
150 K				
Ba1	0.6027 (2)	0.6408 (3)	0.2506 (3)	0.0051 (5)
Ba2	0.1813 (2)	0.5489 (3)	0.2161 (3)	0.0048 (4)
O1	0.8819 (2)	0.4886 (2)	0.1761 (3)	0.0065 (4)
O2	0.4124 (2)	0.3605 (3)	0.1460 (3)	0.0070 (4)
O3	0.6068 (2)	0.3462 (3)	0.4937 (3)	0.0067 (4)
O4	0.1649 (2)	0.2964 (2)	0.4653 (3)	0.0089 (4)
D1	0.8847 (2)	0.5311 (3)	0.3106 (3)	0.0239 (5)
D2	0.4711 (2)	0.3502 (3)	0.2725 (3)	0.0181 (4)
D3	0.6246 (2)	0.2359 (3)	0.4422 (3)	0.0224 (5)
D4	0.1017 (2)	0.2429 (3)	0.5517 (4)	0.0252 (6)
100 K				
Ba1	0.6032 (2)	0.6408 (3)	0.2505 (3)	0.0024 (4)
Ba2	0.1814 (2)	0.5488 (3)	0.2162 (3)	0.0034 (4)
O1	0.8819 (2)	0.4886 (2)	0.1767 (3)	0.0053 (4)
O2	0.4119 (2)	0.3604 (2)	0.1458 (3)	0.0057 (4)
O3	0.6064 (2)	0.3464 (3)	0.4937 (3)	0.0046 (4)
O4	0.1646 (2)	0.2960 (2)	0.4655 (3)	0.0062 (4)
D1	0.8847 (2)	0.5317 (3)	0.3106 (3)	0.0219 (5)
D2	0.4711 (2)	0.3502 (2)	0.2733 (3)	0.0173 (4)
D3	0.6246 (2)	0.2356 (3)	0.4412 (3)	0.0202 (5)
D4	0.1012 (2)	0.2427 (3)	0.5514 (4)	0.0229 (5)
50 K				
Ba1	0.6032 (2)	0.6411 (2)	0.2509 (3)	0.0007 (4)
Ba2	0.1817 (2)	0.5495 (3)	0.2158 (3)	0.0019 (4)
O1	0.8822 (2)	0.4887 (2)	0.1764 (3)	0.0039 (4)
O2	0.4122 (2)	0.3605 (2)	0.1457 (3)	0.0041 (4)
O3	0.6065 (2)	0.3463 (3)	0.4933 (3)	0.0031 (4)
O4	0.1643 (2)	0.2964 (2)	0.4656 (3)	0.0053 (4)
D1	0.8847 (2)	0.5315 (3)	0.3106 (3)	0.0198 (4)
D2	0.4712 (2)	0.3503 (2)	0.2727 (3)	0.0156 (4)
D3	0.6245 (2)	0.2353 (3)	0.4418 (3)	0.0189 (5)
D4	0.1010 (2)	0.2431 (3)	0.5521 (4)	0.0209 (5)
10 K				
Ba1	0.6031 (2)	0.6413 (2)	0.2504 (3)	0.0004 (4)
Ba2	0.1815 (2)	0.5489 (2)	0.2163 (3)	0.0013 (4)
O1	0.8821 (2)	0.4890 (2)	0.1763 (3)	0.0033 (4)
O2	0.4125 (2)	0.3604 (2)	0.1457 (3)	0.0033 (4)
O3	0.6064 (2)	0.3467 (2)	0.4934 (3)	0.0017 (4)
O4	0.1641 (2)	0.2961 (2)	0.4655 (3)	0.0051 (4)
D1	0.8848 (2)	0.5319 (2)	0.3105 (3)	0.0196 (4)
D2	0.4714 (2)	0.3500 (2)	0.2734 (3)	0.0153 (4)
D3	0.6245 (2)	0.2355 (2)	0.4424 (3)	0.0173 (5)
D4	0.1007 (2)	0.2425 (3)	0.5521 (3)	0.0199 (5)

stable. There is a change in coordination numbers and in the number of different barium polyhedra. Furthermore, the relatively straight hydrogen bonds of the β phase are replaced by weak, strongly bent and often bifurcated hydrogen bonds in the high-temperature phase. The structural similarity between the α and the β phase can be found when applying the transformation matrix [2/3, 0, 1/3; −1/3, 0, 1/3; 0, −1, 0] + [0, 1/2, 1/2] to the α phase (Fig. 5). Within the small cell, the $(Ba2)_\beta$ site corresponds to the $(Ba3)_\alpha$ site. The $(Ba1)_\beta$ site splits into $(Ba1)_\alpha$, which occupies a special position on an m plane, and $(Ba2)_\alpha$. The n-glide plane of the β phase corresponds to the a-glide plane of the α phase. The unit-cell volume of the high-temperature α phase is smaller than the comparable volume of the β phase. This is mainly caused by a strong shortening of the c_α axis, which corresponds to the (negative) b_β axis. The density of the high-temperature α

Table 4
Atom positions and atomic displacement parameters of α-$Ba(OD)_2$.

Site	x	y	z	U_{eq}
552 K				
Ba1	0.319 (1)	0.2500	0.444 (1)	0.026 (3)
Ba2	0.4731 (5)	0.3772 (5)	0.9170 (9)	0.023 (2)
Ba3	0.3330 (6)	0.4883 (4)	0.422 (1)	0.024 (2)
O1	0.079 (1)	0.2500	0.373 (2)	0.040 (3)
O2	0.327 (1)	0.2500	0.812 (2)	0.052 (4)
O3	0.4925 (9)	0.3668 (7)	0.528 (1)	0.061 (3)
O4	0.2814 (8)	0.3804 (5)	0.161 (1)	0.047 (3)
O5	0.2130 (6)	0.3963 (4)	0.655 (1)	0.033 (2)
O6	0.0570 (8)	0.4746 (5)	0.299 (1)	0.042 (2)
D1	0.054 (1)	0.2500	0.265 (3)	0.126 (7)
D2	0.268 (1)	0.2500	0.905 (2)	0.081 (5)
D3	0.553(1)	0.3388 (6)	0.495 (1)	0.112 (5)
D4	0.2277 (8)	0.3515 (6)	0.130 (2)	0.109 (5)
D5	0.2356 (6)	0.3556 (5)	0.736 (1)	0.052 (2)
D6	0.0807 (9)	0.4316 (5)	0.246 (1)	0.096 (4)
480 K				
Ba1	0.3171 (8)	0.2500	0.441 (1)	0.021 (2)
Ba2	0.4737 (4)	0.3764 (4)	0.9180 (7)	0.019 (1)
Ba3	0.3338 (5)	0.4883 (3)	0.4249 (9)	0.021 (2)
O1	0.0775 (9)	0.2500	0.376 (1)	0.042 (3)
O2	0.3257 (9)	0.2500	0.814 (1)	0.043 (3)
O3	0.4930 (7)	0.3654 (5)	0.529 (1)	0.046 (2)
O4	0.2809 (6)	0.3803 (4)	0.164 (1)	0.035 (2)
O5	0.2141 (5)	0.3950 (3)	0.6572 (8)	0.027 (2)
O6	0.0574 (7)	0.4756 (4)	0.298 (1)	0.038 (2)
D1	0.055 (1)	0.2500	0.261 (2)	0.131 (6)
D2	0.2683 (9)	0.2500	0.913 (2)	0.077 (4)
D3	0.5542 (8)	0.3390 (5)	0.496 (1)	0.101 (4)
D4	0.2252 (7)	0.3516 (5)	0.127 (1)	0.102 (3)
D5	0.2372 (5)	0.3527 (4)	0.7382 (8)	0.048 (2)
D6	0.0779 (7)	0.4303 (4)	0.246 (1)	0.081 (3)
200 K				
Ba1	0.3185 (6)	0.2500	0.4382 (9)	0.001 (2)
Ba2	0.4771 (4)	0.3766 (3)	0.9157 (6)	0.007 (1)
Ba3	0.3323 (4)	0.4893 (3)	0.4292 (7)	0.005 (1)
O1	0.0758 (7)	0.2500	0.372 (1)	0.012 (2)
O2	0.3212 (8)	0.2500	0.815 (1)	0.031 (2)
O3	0.4975 (5)	0.3646 (3)	0.5226 (7)	0.014 (1)
O4	0.2855 (4)	0.3787 (3)	0.1598 (7)	0.011 (1)
O5	0.2180 (5)	0.3941 (3)	0.6573 (7)	0.009 (1)
O6	0.0567 (5)	0.4763 (3)	0.2922 (7)	0.013 (1)
D1	0.055 (1)	0.2500	0.255 (2)	0.105 (5)
D2	0.2784 (8)	0.2500	0.935 (2)	0.057 (3)
D3	0.5644 (7)	0.3349 (4)	0.512 (1)	0.063 (2)
D4	0.2152 (6)	0.3597 (5)	0.151 (1)	0.076 (2)
D5	0.2377 (4)	0.3474 (3)	0.7409 (7)	0.028 (1)
D6	0.0609 (6)	0.4282 (3)	0.2308 (9)	0.046 (2)
150 K				
Ba1	0.3187 (6)	0.2500	0.4353 (9)	0.0020
Ba2	0.4771 (4)	0.3764 (3)	0.9167 (6)	0.006 (1)
Ba3	0.3324 (4)	0.4890 (3)	0.4305 (7)	0.0013 (9)
O1	0.0762 (6)	0.2500	0.3738 (9)	0.009 (1)
O2	0.3216 (7)	0.2500	0.815 (1)	0.023 (2)
O3	0.4992 (4)	0.3650 (3)	0.5213 (7)	0.010 (1)
O4	0.2872 (4)	0.3788 (3)	0.1619 (7)	0.009 (1)
O5	0.2188 (5)	0.3942 (3)	0.6573 (7)	0.008 (1)
O6	0.0562 (5)	0.4759 (3)	0.2922 (7)	0.012 (1)
D1	0.055 (1)	0.2500	0.259 (2)	0.095 (5)
D2	0.2808 (8)	0.2500	0.939 (1)	0.055 (3)
D3	0.5663 (6)	0.3333 (4)	0.516 (1)	0.058 (2)
D4	0.2129 (6)	0.3616 (5)	0.157 (1)	0.066 (2)
D5	0.2379 (4)	0.3469 (3)	0.7417 (7)	0.024 (1)
D6	0.0579 (6)	0.4279 (3)	0.2274 (8)	0.041 (2)

phase is nevertheless lower than that of the β phase. If one compares the number of formula units per unit cell, a ratio 5:6 = α(552 K):β(480 K) is obtained. The volume per formula unit gives 61.42 for the β phase and 66.19 for the α phase, confirming the usual expansive behaviour with increasing temperature. Considering only the Ba sites within the unit cell, the α phase contains 20 atoms per unit cell, while the β phase contains 24 atoms per unit cell, corresponding to the above-mentioned ratio. The smaller unit-cell volume of the α phase is compensated by the lack of four formula units (Fig. 5).

3.3.2. α–α_m phase. This order–disorder phase transition is typical for the reduction of the vibrational energy at low temperatures, as the D1 atom, which is disordered over two positions at higher temperature, is cooperatively frozen on one of the two positions, thus violating the m plane and reducing the space-group symmetry. α_m-$Ba(OD)_2$ can be perfectly refined in the space group $P2_1/n$ (Fig. 6). The powder data do not allow to distinguish between a centrosymmetric and acentric structure. An only small improvement of the fit of an acentric model does not justify the concomitant doubling of refinable parameters. The residual values are already excellent for a centrosymmetric model. The unit-cell dimensions remain similar to those of the α phase. Due to the reduction of the symmetry, the structure now shows five distinct barium sites, which do not change their coordination. Only small structural changes occur, which do not need high energies for reversion. The O1, O2, D1 and D2 atoms occupy special sites on the m plane in the orthorhombic structural model of the α phase and

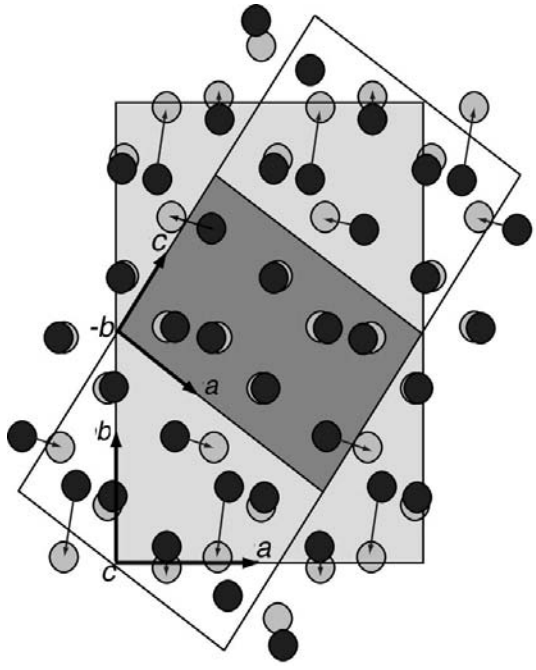

Figure 5
Relationship between the unit cells of β-$Ba(OD)_2$ (smaller and darker one) and α-$Ba(OD)_2$ (large and lighter), shown with the corresponding Ba sites (arrows). The unit cell of the α phase contains four formula units less than the corresponding unit cell of the β phase, which can be seen by the shift of four Ba atoms across the border of the large unit cell.

Table 5
Atom positions and atomic displacement parameters of α_m-Ba(OD)$_2$.

Site	x	y	z	U_{eq}
100 K				
Ba1	0.431 (1)	0.3223 (7)	0.2472 (6)	0.007 (2)
Ba2	0.911 (1)	0.4744 (9)	0.3759 (5)	0.007 (2)
Ba2*a*	0.421 (1)	0.0199 (8)	0.6241 (5)	0.005 (2)
Ba3	0.436 (1)	0.3288 (8)	0.4880 (5)	0.001 (2)
Ba3*a*	0.928 (1)	0.1683 (8)	0.5082 (5)	0.002 (2)
O1	0.378 (1)	0.0747 (7)	0.2479 (6)	0.015 (2)
O2	0.810 (1)	0.3254 (7)	0.2519 (6)	0.019 (2)
O3	0.510 (1)	0.5073 (8)	0.3618 (4)	0.008 (2)
O3*a*	0.031 (1)	0.0016 (9)	0.6328 (5)	0.011 (2)
O4	0.157 (1)	0.2900 (9)	0.3733 (5)	0.011 (2)
O4*a*	0.666 (1)	0.2076 (8)	0.6185 (5)	0.011 (2)
O5	0.659 (1)	0.2235 (8)	0.3931 (5)	0.014 (2)
O5*a*	0.162 (1)	0.2832 (8)	0.6050 (5)	0.010 (2)
O6	0.289 (1)	0.0584 (8)	0.4753 (5)	0.005 (2)
O6*a*	0.798 (1)	0.4476 (7)	0.5227 (4)	0.002 (2)
D1	0.263 (2)	0.0615 (9)	0.2291 (6)	0.049 (3)
D2	0.940 (1)	0.2870 (7)	0.2532 (6)	0.035 (2)
D3	0.541 (1)	0.579 (1)	0.3308 (6)	0.041 (3)
D3*a*	0.014 (1)	0.933 (1)	0.6651 (6)	0.036 (2)
D4	0.180 (1)	0.210 (1)	0.3596 (6)	0.038 (3)
D4*a*	0.653 (1)	0.289 (1)	0.6381 (6)	0.045 (3)
D5	0.736 (1)	0.2388 (8)	0.3460 (5)	0.027 (2)
D5a	0.239 (1)	0.2586 (8)	0.6517 (5)	0.025 (2)
D6	0.221 (1)	0.0474 (8)	0.4273 (5)	0.028 (2)
D6*a*	0.725 (1)	0.4472 (9)	0.5709 (5)	0.039 (3)
50 K				
Ba1	0.4323 (9)	0.3244 (6)	0.2461 (4)	0.006 (2)
Ba2	0.910 (1)	0.4743 (6)	0.3742 (4)	0.004 (2)
Ba2*a*	0.4201 (9)	0.0190 (6)	0.6248 (4)	0.001 (1)
Ba3	0.4331 (9)	0.3287 (7)	0.4869 (4)	0.002 (1)
Ba3*a*	0.9321 (9)	0.1701 (7)	0.5079 (4)	0.001 (2)
O1	0.3737 (9)	0.0752 (5)	0.2484 (4)	0.011 (2)
O2	0.8150 (8)	0.3260 (5)	0.2484 (4)	0.012 (2)
O3	0.5077 (9)	0.5099 (7)	0.3599 (3)	0.006 (2)
O3*a*	0.0305 (8)	0.0006 (6)	0.6307 (4)	0.003 (1)
O4	0.1577 (9)	0.2909 (7)	0.3729 (4)	0.008 (1)
O4*a*	0.6669 (8)	0.2073 (6)	0.6165 (4)	0.003 (1)
O5	0.6584 (8)	0.2253 (6)	0.3916 (4)	0.003 (1)
O5*a*	0.1661 (9)	0.2869 (7)	0.6055 (4)	0.007 (1)
O6	0.2917 (9)	0.0581 (6)	0.4769 (4)	0.005 (1)
O6*a*	0.7918 (9)	0.4509 (6)	0.5240 (4)	0.006 (1)
D1	0.259 (1)	0.0647 (6)	0.2211 (4)	0.033 (2)
D2	0.9360 (9)	0.2876 (6)	0.2565 (4)	0.028 (2)
D3	0.546 (1)	0.5844 (7)	0.3321 (4)	0.034 (2)
D3*a*	0.013 (1)	0.9352 (8)	0.6650 (5)	0.033 (2)
D4	0.183 (1)	0.2077 (7)	0.3590 (4)	0.026 (2)
D4*a*	0.654 (1)	0.2871 (8)	0.6365 (4)	0.032 (2)
D5	0.7358 (9)	0.2400 (6)	0.3431 (4)	0.022 (2)
D5*a*	0.2407 (9)	0.2577 (6)	0.6514 (4)	0.022 (2)
D6	0.2186 (9)	0.0486 (6)	0.4284 (4)	0.020 (2)
D6*a*	0.7201 (9)	0.4487 (6)	0.5718 (4)	0.025 (2)
10 K				
Ba1	0.4333 (9)	0.3245 (6)	0.2463 (4)	0.005 (2)
Ba2	0.9095 (9)	0.4744 (6)	0.3745 (4)	0.002 (1)
Ba2*a*	0.422 (1)	0.0198 (6)	0.6247 (4)	0.003 (1)
Ba3	0.4322 (9)	0.3292 (7)	0.4879 (4)	0.001 (1)
Ba3*a*	0.926 (1)	0.1709 (7)	0.5070 (4)	0.001 (2)
O1	0.3744 (8)	0.0754 (5)	0.2484 (4)	0.006 (1)
O2	0.8147 (8)	0.3241 (5)	0.2483 (4)	0.008 (1)
O3	0.5075 (8)	0.5092 (6)	0.3587 (3)	0.001 (1)
O3*a*	0.0316 (9)	0.0028 (7)	0.6311 (4)	0.008 (2)
O4	0.1586 (9)	0.2910 (7)	0.3727 (4)	0.003 (1)
O4*a*	0.6671 (8)	0.2075 (6)	0.6172 (4)	0.004 (1)
O5	0.6580 (8)	0.2260 (6)	0.3925 (4)	0.004 (1)
O5*a*	0.1652 (8)	0.2885 (7)	0.6059 (4)	0.006 (1)
O6	0.2902 (8)	0.0579 (6)	0.4765 (4)	0.001 (1)
O6*a*	0.7935 (9)	0.4499 (6)	0.5233 (4)	0.004 (1)
D1	0.258 (1)	0.0645 (6)	0.2200 (4)	0.025 (2)

Table 5 (continued)

Site	x	y	z	U_{eq}
D2	0.9405 (9)	0.2877 (6)	0.2562 (4)	0.028 (2)
D3	0.545 (1)	0.5851 (7)	0.3330 (4)	0.027 (2)
D3*a*	0.011 (1)	0.9358 (7)	0.6643 (4)	0.023 (2)
D4	0.1842 (9)	0.2075 (7)	0.3581 (4)	0.022 (2)
D4*a*	0.654 (1)	0.2875 (7)	0.6367 (4)	0.028 (2)
D5	0.7360 (8)	0.2406 (6)	0.3435 (4)	0.019 (1)
D5*a*	0.2394 (9)	0.2567 (6)	0.6523 (4)	0.020 (2)
D6	0.2173 (9)	0.0461 (6)	0.4278 (4)	0.021 (2)
D6*a*	0.7205 (8)	0.4482 (6)	0.5723 (4)	0.022 (2)

therefore form two equivalent hydrogen bonds in different directions. While the D2 atom hardly changes its hydrogen-bond geometry at lower temperatures, the D1 atom begins to be displaced from the *m* plane, which is expressed by a much higher atomic displacement parameter compared with those of the other D atoms (Fig. 7). It appears to dynamically occupy a split position and at even lower temperatures the phase transition occurs when the D1 atom becomes trapped on one of the split positions, and thus violates the *m* plane and forms

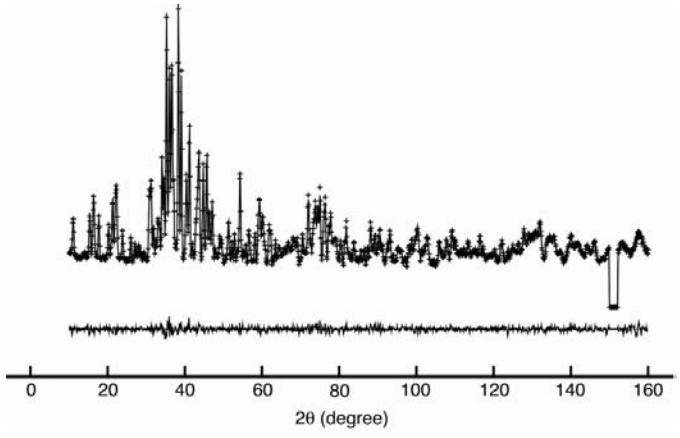

Figure 6
Observed (crosses) and calculated (line) neutron powder diffraction pattern of α_m-Ba(OD)$_2$ and difference plot.

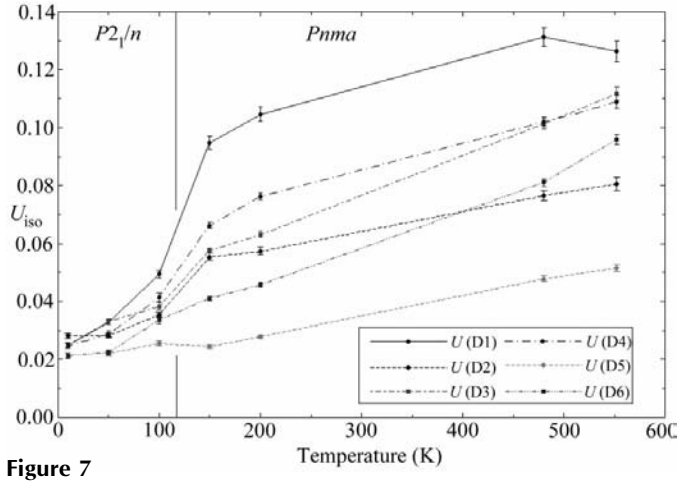

Figure 7
Isotropic atomic displacement parameters of non-equivalent D atoms of α-Ba(OD)$_2$ with temperature.

Table 6
Selected polyhedral bond distances in β-Ba(OD)$_2$.

The average Ba2—O bond distance is given for [7] and [8] coordination. RT = room temperature.

	RT	480 K	420 K	300 K	250 K	200 K	150 K	100 K	50 K	10 K
Ba1—O2	2.665 (6)	2.680 (5)	2.674 (5)	2.676 (3)	2.673 (4)	2.665 (3)	2.670 (3)	2.667 (3)	2.668 (3)	2.665 (3)
Ba1—O3	2.727 (6)	2.739 (4)	2.737 (5)	2.733 (3)	2.740 (3)	2.744 (3)	2.742 (3)	2.740 (3)	2.740 (3)	2.739 (2)
Ba1—O1	2.797 (6)	2.799 (5)	2.801 (6)	2.787 (3)	2.784 (3)	2.784 (3)	2.784 (3)	2.782 (3)	2.779 (3)	2.780 (3)
Ba1—O4	2.828 (6)	2.816 (4)	2.827 (5)	2.805 (3)	2.800 (3)	2.804 (3)	2.800 (3)	2.798 (3)	2.795 (3)	2.800 (3)
Ba1—O3	2.841 (7)	2.842 (5)	2.850 (6)	2.844 (3)	2.843 (3)	2.846 (3)	2.842 (3)	2.839 (3)	2.837 (3)	2.838 (3)
Ba1—O2	2.881 (6)	2.925 (4)	2.909 (5)	2.899 (3)	2.893 (3)	2.888 (3)	2.881 (3)	2.885 (3)	2.884 (3)	2.882 (3)
Ba1—O1	2.994 (6)	3.054 (4)	3.026 (5)	2.994 (3)	2.979 (3)	2.971 (3)	2.964 (3)	2.957 (3)	2.959 (3)	2.957 (2)
Ba1—O4	3.024 (6)	3.075 (4)	3.048 (5)	3.049 (3)	3.046 (3)	3.035 (3)	3.031 (3)	3.029 (3)	3.027 (3)	3.021 (2)
⟨Ba1—O⟩	2.85 (2)	2.87 (1)	2.86 (2)	2.848 (8)	2.845 (9)	2.842 (8)	2.839 (8)	2.837 (8)	2.836 (8)	2.835 (8)
Ba2—O4	2.642 (6)	2.643 (5)	2.640 (5)	2.620 (3)	2.625 (3)	2.620 (3)	2.620 (3)	2.621 (3)	2.625 (3)	2.620 (3)
Ba2—O1	2.688 (7)	2.694 (5)	2.694 (6)	2.683 (3)	2.679 (4)	2.675 (3)	2.675 (3)	2.677 (3)	2.674 (3)	2.676 (3)
Ba2—O2	2.734 (5)	2.711 (4)	2.727 (5)	2.708 (3)	2.705 (3)	2.700 (3)	2.704 (3)	2.697 (3)	2.698 (2)	2.700 (2)
Ba2—O2	2.787 (6)	2.832 (4)	2.807 (5)	2.809 (3)	2.804 (3)	2.806 (3)	2.797 (3)	2.794 (3)	2.791 (3)	2.794 (3)
Ba2—O4	2.790 (6)	2.777 (4)	2.782 (5)	2.788 (3)	2.786 (3)	2.783 (3)	2.780 (3)	2.778 (3)	2.774 (3)	2.778 (3)
Ba2—O3	2.810 (6)	2.783 (5)	2.794 (5)	2.782 (3)	2.778 (3)	2.776 (3)	2.775 (3)	2.774 (3)	2.773 (3)	2.772 (3)
Ba2—O1	2.844 (5)	2.834 (4)	2.842 (5)	2.835 (3)	2.835 (3)	2.833 (3)	2.831 (3)	2.828 (2)	2.828 (2)	2.825 (2)
Ba2—O3	3.517 (6)	3.478 (5)	3.495 (5)	3.493 (3)	3.498 (3)	3.493 (3)	3.496 (3)	3.494 (3)	3.498 (3)	3.497 (3)
⟨Ba2—O⟩ [7]	2.41 (2)	2.41 (1)	2.41 (1)	2.403 (8)	2.402 (8)	2.399 (8)	2.398 (8)	2.396 (8)	2.395 (7)	2.340 (7)
⟨Ba2—O⟩ [8]	2.55 (2)	2.54 (1)	2.55 (2)	2.539 (8)	2.539 (9)	2.536 (8)	2.535 (8)	2.533 (8)	2.533 (8)	2.485 (8)

two unequal hydrogen bonds. Strong bonding occurs for the O1—D1···O3 bond, whereas the O1—D1···O3*a* bond, which has been symmetrically equivalent, becomes very weak and has nearly no influence on the D1 atom (Fig. 8). This effect is even increased towards lower temperatures. The resulting asymmetry is also reflected by a lengthening of the Ba3—O3 bonds compared with the O3*a*—Ba3*a* bonds (Table 7). After the phase transition the isotropic atomic displacement parameter of the D1 atom decreases to about half the value and adapts to those of the other D atoms. These observations confirm the phase transition to be of an order–disorder type. We suggest a dynamic disorder due to the large difference in isotropic atomic displacement parameters and the reasonable explanation of freezing on a split position at low temperature. Nevertheless, the development of isotropic atomic displacement parameters with decreasing temperature shows the same gradient down to the phase transition for the D1 atom as for the other D atoms. This could also indicate a static disorder based on Landau theory (as shown previously for other substances, *e.g.* Boysen, 1992; Boysen & Lerch, 1996; Lehnert *et al.*, 2000), as the gradient of the D1 curve should show a steeper gradient in the case of a dynamic disorder. If looking at a projection along the *b* axis of the α_m phase (Fig. 9), it can easily be seen that all the D1, D2, D3, D3*a*, D4 and D4*a* atoms are arranged within the only polyhedral cavity, which has no Ba atom in the centre. The D atoms are weakly hydrogen-bonded across this void. This cavity is the most flexible part within the structure and shows the strongest distortion by the low-temperature phase transition. The shift of the D1 atom

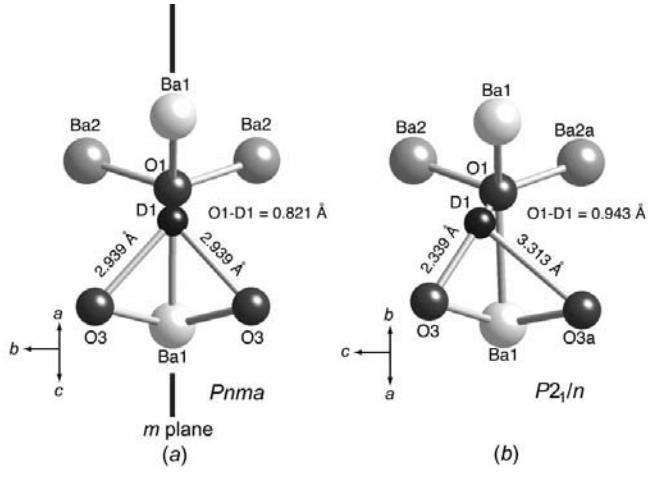

Figure 8
Mechanism of the order–disorder phase transition. The D1 atom violates the *m* plane and hence forms two unequal hydrogen bonds. (*a*) α-Ba(OD)$_2$, (*b*) α_m-Ba(OD)$_2$.

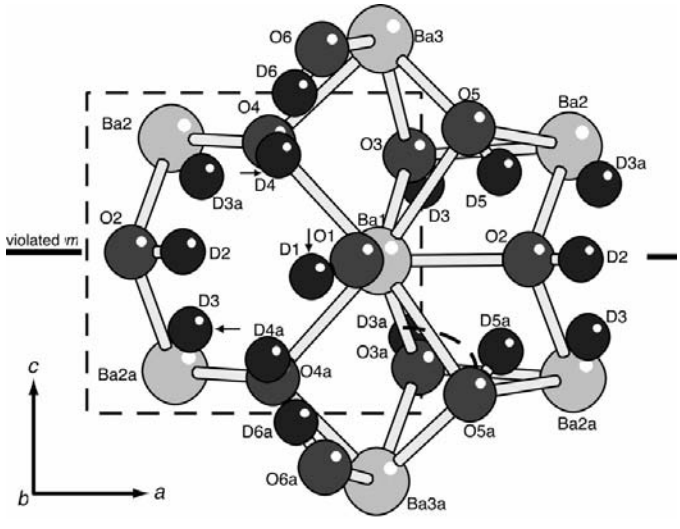

Figure 9
Projection of a thin structural slice along the *a* axis of α_m-Ba(OD)$_2$. An interstitial that holds D1, D2, D3, D3*a*, D4 and D4*a* atoms and the widening Ba1—O3*a*—Ba2*a* angle are indicated by dashed lines. Small arrows show the relative movement of the deuterium sites during the phase transition.

Table 7
Selected polyhedral bond distances in α- und α_m-$Ba(OD)_2$.

The average Ba1—O bond distance, ⟨Ba1—O⟩, is given for [8] and [9] coordination, ⟨Ba2—O⟩ for [7] amd [8].

	552 K	480 K	200 K	150 K	100 K	50 K	10 K
Ba1—O2	2.63 (2)	2.66 (1)	2.67 (1)	2.69 (1)	2.70 (1)	2.710 (8)	2.701 (8)
Ba1—O1	2.71 (2)	2.70 (1)	2.71 (1)	2.693 (9)	2.73 (1)	2.742 (8)	2.740 (8)
Ba1—O3 (2×)	2.81 (1)	2.81 (1)	2.786 (7)	2.800 (7)	2.81 (1)	2.794 (9)	2.771 (9)
Ba1—O3*a*					2.79 (1)	2.786 (9)	2.77 (1)
Ba1—O4 (2×)	3.00 (1)	2.955 (9)	2.913 (6)	2.886 (6)	2.89 (1)	2.906 (9)	2.902 (9)
Ba1—O4*a*					2.82 (1)	2.829 (9)	2.826 (9)
Ba1—O5 (2×)	3.098 (9)	3.078 (8)	3.037 (6)	3.044 (6)	3.06 (1)	3.044 (9)	3.045 (9)
Ba1—O5*a*					3.10 (1)	3.118 (9)	3.116 (9)
Ba1—O1	3.67 (2)	3.66 (1)	3.58 (1)	3.570 (9)	3.52 (1)	3.486 (9)	3.493 (8)
⟨Ba1—O⟩, [8]	2.89 (4)	2.88 (3)	2.86 (2)	2.86 (2)	2.86 (3)	2.87 (2)	2.86 (3)
⟨Ba1—O⟩, [9]	2.98 (4)	2.97 (3)	2.94 (2)	2.93 (2)	2.93 (3)	2.94 (3)	2.93 (3)
Ba2—O6*a*	2.63 (1)	2.625 (9)	2.598 (7)	2.605 (7)	2.57 (1)	2.630 (9)	2.611 (9)
Ba2—O5*a*	2.735 (9)	2.735 (7)	2.710 (7)	2.716 (7)	2.71 (2)	2.67 (1)	2.65 (1)
Ba2—O4	2.75 (1)	2.764 (8)	2.722 (6)	2.709 (6)	2.66 (1)	2.66 (1)	2.66 (1)
Ba2—O6*a*	2.76 (1)	2.767 (9)	2.779 (7)	2.768 (7)	2.76 (1)	2.787 (9)	2.786 (9)
Ba2—O2	2.77 (1)	2.764 (8)	2.786 (8)	2.779 (7)	2.69 (1)	2.695 (9)	2.712 (9)
Ba2—O3	2.79 (1)	2.783 (9)	2.798 (7)	2.814 (7)	2.87 (1)	2.878 (9)	2.878 (8)
Ba2—O1	2.85 (1)	2.807 (9)	2.786 (7)	2.771 (6)	2.77 (1)	2.785 (9)	2.788 (9)
Ba2—O5	3.459 (9)	3.439 (7)	3.394 (7)	3.386 (7)	3.28 (1)	3.256 (9)	3.252 (9)
⟨Ba2—O⟩, [7]	2.76 (3)	2.75 (2)	2.74 (2)	2.74 (2)	2.72 (2)	2.73 (2)	2.73 (2)
⟨Ba2—O⟩, [8]	2.85 (3)	2.84 (2)	2.82 (2)	2.82 (2)	2.79 (3)	2.80 (3)	2.79 (3)
Ba2*a*—O6					2.63 (1)	2.611 (9)	2.621 (9)
Ba2*a*—O4*a*					2.69 (1)	2.698 (9)	2.684 (9)
Ba2*a*—O1					2.72 (1)	2.717 (9)	2.712 (9)
Ba2*a*—O5					2.73 (1)	2.726 (9)	2.745 (9)
Ba2*a*—O3*a*					2.78 (1)	2.770 (8)	2.776 (9)
Ba2*a*—O6					2.78 (1)	2.796 (9)	2.791 (9)
Ba2*a*—O2					2.82 (1)	2.754 (9)	2.767 (9)
Ba2*a*—O5*a*					3.42 (1)	3.43 (1)	3.45 (1)
⟨Ba2*a*—O⟩, [7]					2.73 (3)	2.73 (2)	2.73 (2)
⟨Ba2*a*—O⟩, [8]					2.82 (3)	2.81 (3)	2.82 (3)
Ba3—O5	2.63 (1)	2.626 (8)	2.575 (7)	2.558 (7)	2.52 (1)	2.526 (9)	2.528 (9)
Ba3—O4	2.66 (1)	2.694 (9)	2.683 (7)	2.670 (7)	2.74 (1)	2.705 (9)	2.710 (9)
Ba3—O5*a*	2.76 (1)	2.771 (8)	2.772 (7)	2.780 (7)	2.80 (1)	2.784 (9)	2.775 (9)
Ba3—O3	2.80 (1)	2.80 (1)	2.815 (7)	2.810 (6)	2.90 (1)	2.93 (1)	2.945 (9)
Ba3—O6*a*	2.96 (1)	2.95 (1)	2.900 (7)	2.893 (7)	2.92 (1)	2.88 (1)	2.89 (1)
Ba3—O6*a*	3.02 (1)	2.98 (1)	2.928 (7)	2.923 (7)	2.95 (1)	2.919 (9)	2.922 (9)
Ba3—O4*a*	3.05 (1)	3.046 (9)	3.007 (6)	3.018 (6)	2.98 (1)	2.976 (9)	2.979 (9)
Ba3—O3	3.12 (1)	3.11 (1)	3.062 (7)	3.044 (6)	3.07 (1)	3.090 (9)	3.094 (9)
Ba3—O6	3.20 (1)	3.20 (1)	3.185 (7)	3.188 (7)	3.13 (1)	3.11 (1)	3.12 (1)
⟨Ba3—O⟩	2.91 (3)	2.91 (3)	2.88 (2)	2.88 (2)	2.89 (3)	2.88 (3)	2.89 (3)
Ba3*a*—O5*a*					2.60 (1)	2.610 (9)	2.650 (9)
Ba3*a*—O4*a*					2.65 (1)	2.651 (9)	2.637 (9)
Ba3*a*—O5					2.73 (1)	2.758 (9)	2.708 (9)
Ba3*a*—O3*a*					2.82 (1)	2.809 (9)	2.83 (1)
Ba3*a*—O6					2.89 (1)	2.879 (9)	2.912 (9)
Ba3*a*—O6					2.93 (1)	2.96 (1)	2.94 (1)
Ba3*a*—O3*a*					2.98 (1)	2.954 (9)	2.97 (1)
Ba3*a*—O4					3.07 (1)	3.059 (9)	3.076 (9)
Ba3*a*—O6*a*					3.19 (1)	3.22 (1)	3.19 (1)
⟨Ba3*a*—O⟩					2.87 (3)	2.88 (3)	2.88 (3)

away from the mirror plane also influences the D3, D3*a* and D4 atoms to shift and violate the mirrored structural arrangement. Changes of the weak bi- and trifurcated hydrogen bonds of these D atoms occur. In addition, the Ba2—O4—Ba1 and O2—Ba2*a*—O4a angles increase, while the Ba2*a*—O4*a*—Ba1 angle decreases in the low-temperature α_m phase. The interstitial is distorted in such a way that the Ba1—O3*a*—Ba2*a* angle also increases. In this sense, the increasing monoclinic β angle and the increasing *a* and *c* axes of the α_m phase can be explained. The distortion of the cavity and the strengthening of the O1—D1···O3 bond, which points to the direction of the *b* axis within the (100) plane, are accompanied by a compression of the structural framework along the *b* axis.

3.4. Hydrogen bonds

3.4.1. β-$Ba(OD)_2$. The hydrogen-bonding scheme within the β phase is very simple and straightforward. Each of the four O atoms forms one hydrogen bond and serves once as a donor and once as an acceptor. It is an undulated, homodrome system with a mean O—D distance of 0.959 (6) Å, O—O of 3.011 (6) Å and O—D···O angle of 163.2 (5)° at 300 K. At decreasing temperature the hydrogen-bond strength increases. This is evidenced by a uniform increase in O—D distances (Table 8) and parallel to it by a uniform decrease of the O—O distances. The O1—D1···O4 and O4—D4···O2 angles are not sensitive to changes in temperature, while the O2—D2···O3 angle slightly decreases and the O3—D3···O1 angle increases with decreasing temperature.

3.4.2. α-$Ba(OD)_2$. As we can expect, the hydrogen bonds in the high-temperature α phase are weaker, stronger bent and often bifurcated, due to the lower density. The mean O—D distance shrinks to 0.907 Å, the O—O distances increase and the O—D···O angle is reduced to less than 155.8° at 200 K. The influence of hydrogen bonding within the whole structural arrangement is decreased and only very weak D···O interactions exist in most cases. The D atoms are strongly bonded within their O—D group (Table 9). At high temperature the D1 and D2 atoms show a bifurcation with symmetry. The D3 atom shows a very weak single and the D4 atom a bifurcated O—D···O interaction (Table 10). The D5 atom is part of a single and the D6 atom of a symmetrically bifurcated hydrogen bond. With decreasing temperature towards the α–α_m phase transition, these interactions and hydrogen bonds gain in strength as the O—O and D···O distances decrease significantly. In most cases this is correlated with an increasing O—D···O angle (except O1—D1···O3, which barely decreases, and O3—D3···O4, which is inversely correlated with the increasing angle of one of the O4—D4···O3 bonds in this O3—D3···D4—O4 arrangement). The only exception is

Table 8
Hydrogen bonds (Å) and angles (°) in β-Ba(OD)$_2$.

RT = room temperature.

	O1—D1···O4			O2—D2···O3		
T (K)	O1—D1	O1—O4	O1—D1···O4	O2—D2	O2—O3	O2—D2···O3
RT	0.957 (7)	3.037 (6)	155.2 (5)	0.967 (6)	2.836 (6)	171.7 (4)
480	0.948 (6)	3.090 (5)	156.1 (4)	0.956 (5)	2.923 (5)	172.4 (3)
420	0.954 (6)	3.071 (6)	155.2 (4)	0.952 (5)	2.884 (5)	172.1 (4)
300	0.962 (3)	3.046 (3)	155.6 (2)	0.972 (3)	2.861 (3)	171.2 (2)
250	0.967 (3)	3.035 (3)	155.3 (2)	0.971 (3)	2.847 (3)	171.0 (2)
200	0.966 (3)	3.031 (3)	155.4 (2)	0.977 (3)	2.840 (3)	170.7 (2)
150	0.966 (3)	3.024 (3)	155.0 (2)	0.973 (3)	2.829 (3)	170.8 (2)
100	0.964 (3)	3.019 (3)	155.3 (2)	0.980 (3)	2.829 (3)	170.9 (2)
50	0.964 (3)	3.016 (3)	155.3 (2)	0.976 (3)	2.826 (3)	170.9 (2)
10	0.965 (3)	3.016 (3)	155.3 (2)	0.979 (3)	2.823 (2)	170.5 (2)

	O3—D3···O1			O4—D4···O2		
T (K)	O3—D3	O3—O1	O3—D3···O1	O4—D4	O4—O2	O4—D4···O2
RT	0.956 (7)	3.062 (6)	166.7 (4)	0.932 (7)	3.047 (6)	160.6 (6)
480	0.920 (6)	3.127 (5)	166.7 (4)	0.925 (5)	3.097 (4)	158.8 (4)
420	0.936 (6)	3.092 (6)	167.1 (4)	0.928 (6)	3.077 (5)	159.1 (5)
300	0.947 (3)	3.080 (3)	167.7 (2)	0.956 (3)	3.058 (3)	158.4 (3)
250	0.955 (3)	3.071 (3)	167.8 (2)	0.959 (3)	3.044 (3)	159.1 (3)
200	0.957 (3)	3.057 (3)	168.1 (2)	0.965 (3)	3.036 (3)	158.7 (2)
150	0.956 (3)	3.047 (3)	168.3 (2)	0.968 (3)	3.030 (3)	159.1 (2)
100	0.962 (3)	3.047 (3)	168.2 (2)	0.966 (3)	3.026 (2)	159.3 (2)
50	0.961 (3)	3.043 (3)	168.3 (2)	0.968 (3)	3.021 (2)	159.0 (2)
10	0.961 (3)	3.043 (3)	168.2 (2)	0.969 (3)	3.015 (2)	159.0 (2)

Table 9
O—D distances (Å) in α- and α_m-Ba(OD)$_2$.

T (K)	O1—D1	O2—D2	O3—D3	O3*a*—D3*a*	O4—D4	O4*a*—D4*a*	O5—D5	O5*a*—D5*a*	O6—D6	O6*a*—D6*a*
552	0.82 (2)	0.94 (2)	0.85 (2)		0.80 (1)		0.93 (1)		0.85 (1)	
480	0.86 (2)	0.95 (1)	0.84 (1)		0.82 (1)		0.944 (8)		0.87 (1)	
200	0.86 (2)	0.97 (1)	0.884 (9)		0.835 (8)		0.993 (7)		0.903 (7)	
150	0.85 (1)	0.99 (1)	0.901 (8)		0.863 (8)		1.002 (7)		0.911 (7)	
100	0.88 (1)	1.02 (1)	0.96 (1)	0.93 (1)	0.91 (1)	0.95 (1)	0.97 (1)	0.97 (1)	0.93 (1)	0.96 (1)
50	0.93 (1)	0.960 (8)	0.97 (1)	0.92 (1)	0.95 (1)	0.93 (1)	0.990 (9)	0.965 (9)	0.946 (9)	0.946 (9)
10	0.943 (9)	0.981 (8)	0.97 (1)	0.92 (1)	0.96 (1)	0.93 (1)	1.000 (9)	0.979 (9)	0.951 (9)	0.968 (9)

shown by one of the two bifurcated hydrogen bonds of the D6 atom. As the O6—D6···O3 hydrogen bond becomes quite dominant and strong, the O6—D6···O4 hydrogen bond loses its influence and becomes quite weak. This is in the same way correlated with the formation of a new and very weak O4—D4···O6 hydrogen bond, which makes the D4 atom hydrogen bonded in a trifurcated way. This correlation is due to the D4—D6 repulsion within the O4—D4···D6—O6 arrangement, which reduces the O—D···O angles.

3.4.3. α_m-Ba(OD)$_2$. After the phase transition the new α_m phase shows an even more complex hydrogen-bonding system. As mentioned above, the D1 atom strongly prefers one hydrogen bond towards the O3 atom, while the other one nearly loses all of its influence. In a similar way the D2 atom now begins to prefer the hydrogen bond towards the O4 atom, which gains in strength, while the other one towards the O4*a* atom successively weakens. With further decreasing temperature these differences increase in both the D1 and the D2 atom arrangements. The O3*a*—D3*a*···D4—O4 arrangement becomes more symmetric concerning the O—D···O angles, while the O3—D3···D4*a*—O4*a* arrangement shows increasing asymmetry, as the O4*a*—D4*a*···O3 hydrogen bond is straightened (Table 10). While the O3—D3···O4*a* hydrogen-bond strength is weaker after the phase transition, a new weak O3—D3···O5*a* hydrogen bond is formed, making the D3 atom hydrogen bonded in a bifurcated way. The behavior between the D5, D6 and the new D5*a* and D6*a* atoms does not change much with symmetry reduction. At decreasing temperature the D5/D5*a* atoms become stronger hydrogen bonded and the bifurcation of the D6/D6*a* hydrogen-bonded atoms becomes more and more unequal, as the O3*a*/O3 atoms are preferred as acceptors. The further correlation in the O4*a*—D4*a*···D6*a*—O6*a* and O4—D4···D6—O6 environments can be seen even within only small changes.

3.5. Thermal expansion

The thermal expansion of β-Ba(OD)$_2$ was calculated from ten temperature data points. The least-squares analysis of the

Table 10
O—O distances (Å) and O—D···O angles (°) in α- and α_m-$Ba(OD)_2$.

	552 K		480 K		200 K		150 K	
Hydrogen bond	O—O	O—D···O	O—O	O—D···O	O—O	O—D···O	O—O	O—D···O
O1—D1···O3	3.60 (1)	138.5 (3)	3.59 (1)	138.7 (3)	3.474 (8)	137.6 (2)	3.476 (7)	137.7 (2)
O2—D2···O4	3.35 (1)	114.7 (6)	3.34 (1)	116.0 (5)	3.253 (8)	120.8 (4)	3.260 (8)	121.3 (3)
O3—D3···O4	3.49 (1)	133 (1)	3.48 (1)	134.5 (9)	3.423 (7)	127.9 (6)	3.419 (6)	124.5 (6)
O4—D4···O6					3.124 (7)	107.1 (7)	3.130 (7)	110.8 (7)
O4—D4···O3	3.49 (1)	138 (1)	3.48 (1)	134.0 (9)	3.423 (7)	147.9 (8)	3.419 (6)	147.7 (7)
O4—D4···O1	3.48 (1)	127 (1)	3.47 (1)	123.8 (9)	3.467 (7)	133.9 (7)	3.473 (7)	133.7 (7)
O5—D5···O2	2.97 (1)	154.7 (8)	2.928 (8)	156.0 (7)	2.852 (7)	155.8 (6)	2.849 (6)	155.4 (6)
O6—D6···O3	3.03 (1)	127 (1)	3.05 (1)	129.0 (8)	2.959 (7)	142.7 (6)	2.937 (7)	145.6 (6)
O6—D6···O4	3.11 (1)	133 (1)	3.09 (1)	129.1 (8)	3.124 (7)	114.1 (6)	3.130 (7)	111.5 (6)

	100 K		50 K		10 K	
Hydrogen bond	O—O	O—D···O	O—O	O—D···O	O—O	O—D···O
O1—D1···O3	3.34 (1)	162.5 (9)	3.279 (9)	170.1 (7)	3.273 (8)	170.9 (7)
O1—D1···O3*a*	3.62 (1)	114 (1)	3.617 (9)	102.9 (6)	3.630 (9)	102.1 (6)
O2—D2···O4	3.16 (1)	124.3 (8)	3.163 (9)	131.1 (7)	3.164 (9)	131.1 (7)
O2—D2···O4*a*	3.39 (1)	121.1 (8)	3.359 (8)	113.9 (6)	3.352 (8)	114.7 (6)
O3—D3···O4*a*	3.37 (1)	112.1 (8)	3.34 (1)	111.6 (6)	3.345 (9)	113.5 (6)
O3*a*—D3*a*···O4	3.45 (1)	129.7 (8)	3.44 (1)	127.4 (8)	3.47 (1)	129.7 (7)
O3—D3···O5*a*	3.30 (1)	114.9 (8)	3.24 (1)	118.4 (6)	3.238 (9)	119.7 (6)
O4—D4···O6	3.16 (1)	118.2 (9)	3.19 (1)	117.6 (6)	3.18 (1)	117.0 (6)
O4*a*—D4*a*···O6*a*	3.20 (1)	108.1 (8)	3.189 (9)	108.9 (6)	3.193 (9)	108.9 (6)
O4—D4···O3*a*	3.45 (1)	133.6 (9)	3.44 (1)	132.0 (7)	3.47 (1)	131.4 (6)
O4*a*—D4*a*···O3	3.37 (1)	151.4 (8)	3.34 (1)	152.0 (7)	3.345 (9)	152.7 (7)
O4—D4···O1	3.51 (1)	140.0 (9)	3.489 (9)	140.1 (7)	3.485 (9)	140.8 (7)
O4*a*—D4*a*···O1	3.50 (1)	130.8 (8)	3.506 (9)	131.8 (7)	3.497 (9)	131.3 (6)
O5—D5···O2	2.80 (1)	155 (1)	2.844 (9)	155.8 (7)	2.847 (9)	156.3 (7)
O5*a*—D5*a*···O2	2.87 (1)	159 (1)	2.831 (9)	161.8 (7)	2.825 (9)	163.6 (7)
O6—D6···O3*a*	2.93 (1)	149.7 (9)	2.925 (9)	150.4 (7)	2.927 (9)	150.7 (7)
O6*a*—D6*a*···O3	2.96 (1)	153.5 (9)	2.917 (9)	154.1 (7)	2.949 (8)	154.2 (7)
O6—D6···O4	3.16 (1)	103.0 (8)	3.19 (1)	104.3 (6)	3.18 (1)	102.4 (6)
O6*a*—D6*a*···O4*a*	3.20 (1)	109.0 (9)	3.189 (9)	109.0 (6)	3.193 (9)	108.8 (6)

temperature dependence of the lattice parameters using second-order polynomials gives the following

$$a = 9.3474\ (6) + 4.4\ (6) \times 10^{-5}T + 5.2\ (1) \times 10^{-7}T^2$$
$$b = 7.862\ (2) + 6.8\ (1.8) \times 10^{-5}T + 2.6\ (4) \times 10^{-7}T^2$$
$$c = 6.7511\ (8) + 3.2\ (8) \times 10^{-5}T + 1.4\ (2) \times 10^{-7}T^2$$
$$V = 493.7\ (2) + 8.7\ (1.8) \times 10^{-3}T + 5.4\ (4) \times 10^{-5}T^2,$$

where the temperature is in K. Using these expressions the instantaneous isobaric thermal expansion can be approximated as $\alpha_x = (1/x_0)(\partial x/\partial T)_p$, where x_0 is a reference lattice constant at T_0 (273.16 K). The values are $\alpha_1 = 34.9\ (6) \times 10^{-6}$, $\alpha_2 = 27\ (2) \times 10^{-6}$, $\alpha_3 = 16\ (1) \times 10^{-6}$, $\alpha_{vol} = 76\ (4) \times 10^{-6}$.

Experiment No. 5-24-84 was sponsored by the ILL facilities. A. Friedrich was financially supported by the Swiss National Science Foundation (Credit 21-052682.97 to M. Kunz).

References

Bärnighausen, H., Denzinger, W. & Zeiske, T. (1997). *Z. Kristallogr.* Suppl. 12, 212.
Boysen, H. (1992). *NIST Special Publ. Washington*, **846**, 165–174.
Boysen, H. & Lerch, M. (1996). *Phase Transit.* **59**, 1–24.
Buck, P. & Bärnighausen, H. (1968). *Acta Cryst.* B**24**, 1705–1706.
Cordfunke, E. H. P., Booij, A. S., Konings, R. J. M., van der Laan, R. R., Smit-Groen, V. M. & van Vlaanderen, P. (1996). *Thermochim. Acta*, **273**, 1–9.
Denzinger, W. (1997). Ph.D. thesis. Universität Karlsruhe, Germany.
Friedrich, A., Kunz, M., Miletich, R. & Pattison, P. (2001). In preparation.
Habashy, G. M. & Kolta, G. A. (1972). *J. Inorg. Nucl. Chem.* **34**, 57–67.
Konings, R. J. M., Cordfunke, E. H. P. & Ouweltjes, W. (1988). *J. Chem. Thermodyn.* **20**, 989–992.
Konings, R. J. M., Cordfunke, E. H. P., Shaviv, R. & Westrum E. F. Jr (1990). *Thermochim. Acta*, **157**, 307–314.

Larson, A. C. & Von Dreele, R. B. (1994). Report LAUR86-748. Los Alamos National Laboratory, Los Alamos, New Mexico, USA.
Lehnert, H., Boysen, H., Schneider, J., Frey, F., Hohlwein, D., Radaelli, P. & Ehrenberg, H. (2000). *Z. Kristallogr.* **215**, 536–541.
Lüke, H. (1973). Ph.D. thesis. Universität Karlsruhe, Germany.
Lutz, H. D., Eckers, W., Christian, H. & Engelen, B. (1981). *Thermochim. Acta*, **44**, 337–343.
Lutz, H. D., Eckers, W., Schneider, G. & Haeuseler, H. (1981). *Spectrochim. Acta A*, **37**, 561–567.
Lutz, H. D., Heider, R. & Becker, R.-A. (1969). *Z. Naturforsch. Teil B*, **24**, 1657–1658.
Maneva-Petrova, M. & Nikolova, D. (1985). *Thermochim. Acta*, **92**, 287–291.
Michaud, M. (1968). *Rev. Chim. Miner.* **5**, 89–125.